




Emergence of skyrmionium in a two-dimensional CrGe(Se,Te)₃ Janus monolayerYun Zhang ^{1,2,*}, Changsong Xu ^{2,*}, Peng Chen ², Yousra Nahas,² Sergei Prokhorenko,² and Laurent Bellaïche^{2,†}¹*Department of Physics and Information Technology, Baoji University of Arts and Sciences, Baoji 721016, China*²*Physics Department and Institute for Nanoscience and Engineering, University of Arkansas, Fayetteville, Arkansas 72701, USA*

(Received 3 August 2020; revised 8 October 2020; accepted 23 November 2020; published 10 December 2020)

Utilization of van der Waals magnetic materials as the host of topologically protected skyrmionic and other complex spin textures has been drawing increasing attention. Here, using first-principles-based calculations, we predict a new stable magnetic CrGe(Se,Te)₃ Janus monolayer with a strong Dzyaloshinskii-Moriya interaction (DMI), due to the breaking of inversion symmetry. Consequently, nanometric skyrmions (that carry a topological charge of ± 1) and skyrmionium states (with a zero topological charge) can spontaneously form in the absence of magnetic field. We further unveil a subtle competition between DMI and frustration as key for stabilizing skyrmioniums.

DOI: [10.1103/PhysRevB.102.241107](https://doi.org/10.1103/PhysRevB.102.241107)

Since it was first observed a decade ago [1], magnetic skyrmions, showing whirl-like spin texture with nontrivial topology, have attracted increasing interest due to their potential in future magnetic data storage and spintronics applications [2–5]. Their topological nature of structure provides a great stability even for small sizes. Such skyrmions also, however, experience the skyrmion Hall effect (SHE), in which current-driven skyrmions feel a transverse deflection towards the edge of the racetrack, therefore leading to the annihilation of the skyrmion [6–8]. Interestingly, the deflection direction of magnetic topological defects depends on the sign of the topological charge ($Q = \pm 1$ for the skyrmion). Consequently, spin states that are the combinations of two skyrmions with opposite topological charges results in a total $Q = 0$ and are thus totally free of the SHE. The antiferromagnetic skyrmion [9,10] and the skyrmionium [11–14] are two examples of such spin states. Very recently, the synthetic antiferromagnetic skyrmions have been experimentally reported in magnetic thin films [10]. Similarly, skyrmionium, which is also named “target skyrmion,” has been experimentally observed in nanodisks of the chiral magnet FeGe [12] and in thin NiFe ferromagnetic films grown on top of a topological insulator [13]. However, its size is over 100 nm in both cases, which is not technologically desired. Consequently, finding new skyrmionium with smaller size in other materials will be an important breakthrough. Understanding what governs the formation and stability of such hypothetical new skyrmionium should also advance fundamental knowledge.

In particular, one may wonder if a particular class of materials can host skyrmionium. This class is made of two-dimensional (2D) van der Waals (vdW) materials, such as CrI₃ [15], CrGeTe₃ [16], and Fe₃GeTe₂ [17]. Recently, the discovery of magnetism in these systems provided an

alternative avenue for exploring new exotic spin phenomena with potential applications in the development of novel spintronics devices. Importantly, several theoretical and experimental studies indeed demonstrated the emergence of magnetic skyrmions in 2D vdW materials and their heterostructures, which should stimulate more research efforts on potential novel skyrmion-hosting materials in the emerging arena of vdW 2D magnets [18–25].

Particularly, 2D Janus materials with intrinsic breaking of inversion symmetry have been predicted to be promising candidates for exhibiting magnetic skyrmionic state [18–20]. Such Janus monolayers should be experimentally feasible, since the transition-metal dichalcogenides MoSSe have been already grown using different methods [26,27]. Following this line of thought, we propose here a new kind of 2D Janus CrGe(Se, Te)₃ monolayer [as shown in Fig. 1(a)]. As we will show, exhibiting a strong Dzyaloshinskii–Moriya interaction (DMI) and magnetocrystalline anisotropy (MCA), the CrGe(Se, Te)₃ monolayer can host several exotic magnetic configurations, especially the magnetic skyrmionium, which is the first report of intrinsic skyrmionium appearance in 2D magnetic materials. Particularly, we demonstrate that it is the competition between DMI and exchange frustration that leads to the stabilization of the skyrmionium.

Figure 1(a) depicts the 2D Janus CrGe(Se, Te)₃ monolayers we investigate here. The top atomic layer is formed by the heavier elements Te, while the lighter ions Se are on the bottom layers. Note that, as shown in Fig. 1(b), the density-functional theory (DFT) calculations [see the Supplemental Materials (SM) [28] for details] we performed demonstrate that such system is dynamically stable, since all its phonons have real frequencies. Moreover, additional DFT calculations reveal that the formation energy E_f of CrGe(Se, Te)₃, which is calculated as the energy difference between the total energy of the Janus structure and the sum of the energies per corresponding elementary bulk phases, is found to be -0.86 eV and thus about half that of the pristine CrGeTe₃ (-1.61 eV) compound. These results suggest that

*Y.Z. and C.X. contributed equally to this work.

†laurent@uark.edu

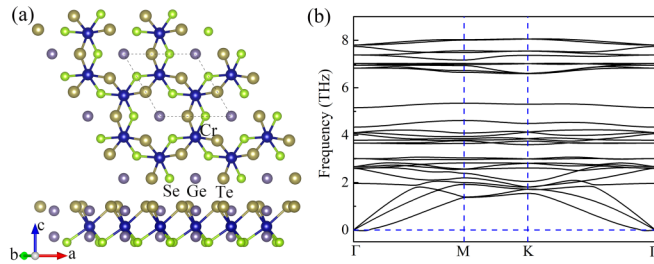


FIG. 1. (a) The top and side views of $\text{CrGe}(\text{Se}, \text{Te})_3$ monolayer. (b) The calculated phonon dispersion of such Janus monolayer.

the presently proposed Janus structure is chemically stable as well.

It is also important to realize that the asymmetry between the top and bottom layers in $\text{CrGe}(\text{Se}, \text{Te})_3$ breaks the inversion symmetry, thus allowing for the DMI interaction between the Cr ions. In fact, understanding the salient features of magnetism in $\text{CrGe}(\text{Se}, \text{Te})_3$ requires a deep knowledge of various magnetic interactions between the Cr ions. For that, we have parametrized the spin-dependent part of the ground-state electronic energy using the following magnetic Hamiltonian:

$$H = H^{\text{EX}} + H^{\text{DMI}} + H^{\text{MCA}}, \quad (1)$$

with

$$\begin{aligned} H^{\text{EX}} &= \frac{1}{2} \sum_{\langle i, j \rangle} J_{ij} \mathbf{S}_i \cdot \mathbf{S}_j, \\ H^{\text{DMI}} &= \frac{1}{2} \sum_{\langle i, j \rangle} \mathbf{D}_{ij} \cdot (\mathbf{S}_i \times \mathbf{S}_j), \\ H^{\text{MCA}} &= \sum_i K_u (\mathbf{S}_i \cdot \hat{\mathbf{z}})^2, \end{aligned} \quad (2)$$

where the first term characterizes exchange coupling and the second term is the DMI interaction, both of them running over all first and second nearest-neighbor (NN) Cr pairs. According to Moriya's rule [29], the D_1 vector of $\text{CrGe}(\text{Se}, \text{Te})_3$ is perpendicular to the Cr_2SeTe plane, which is exactly what we numerically found and which thus testifies to the accuracy of our calculations. Moreover, the D_2 vector is basically pointing from the bridging Se to the Te ions. The third term represents the uniaxial magnetocrystalline anisotropy (MCA) that runs over all Cr sites. These coefficients are listed in Table I and are extracted from DFT calculations and the four-state energy

TABLE I. Magnetic parameters of CrGeTe_3 and $\text{CrGe}(\text{Se}, \text{Te})_3$ monolayers. Note that $S = 3/2$ is used when extracting the magnetic parameters. The units of energy unit are meV.

Mag. para.	CrGeTe_3	$\text{CrGe}(\text{Se}, \text{Te})_3$
J_1	-6.141	-3.267
D_1	0	0.710
D_1/J_1	0	0.217
J_2	0.077	0.476
D_2	0.308	0.249
D_2/J_2	4.000	0.523
K_u	-0.085	-0.420

mapping method (see SM [28] for details). For comparison, we also calculated the magnetic parameters for the prototype CrGeTe_3 , which has no finite D_1 but shows non-negligible D_2 values (where subscripts “1” and “2” refer to first NN and second NN, respectively)—as is consistent with the Moriya's rule [29]. Despite its considerable $|D_2/J_2|$ ratio of 4, we find that the ground state of CrGeTe_3 is (homogeneously) ferromagnetic (FM) due to the large J_1 . We also found that, due to the smaller atomic radius of Se ion with respect to that of Te, the lattice constant of $\text{CrGe}(\text{Se}, \text{Te})_3$ (6.48 Å) decreases as compared with that of the pristine CrGeTe_3 phase (6.73 Å). Consequently, such lattice shrinking reduces the magnitude of the first NN exchange coefficient J_1 , which, by itself, will favor a FM ground state—similar to the Janus monolayers of $\text{Cr}(\text{I}, \text{X})_3$ ($X = \text{Br}, \text{Cl}$) and manganese dichalcogenides [18–20]. However, the now-symmetry-allowed D_1 has a rather large value of 0.71 meV. The resulting large $|D_1/J_1|$ ratio of 0.217 should thus be highly beneficial for generating skyrmionic phases [30,31]. Note, however, that the second NN exchange coefficient J_2 of $\text{CrGe}(\text{Se}, \text{Te})_3$ favors antiferromagnetic (AFM) ordering, which competes with J_1 and therefore results in some frustration. Actually, a number of studies have suggested that skyrmions can be further stabilized in magnetic systems with frustrated exchange interactions [32–34]. We further found that the Janus monolayer $\text{CrGe}(\text{Se}, \text{Te})_3$ favors a strong out-of-plane anisotropy of -0.42 meV/Cr, as a consequence of an interplay between the single ion anisotropy and Kitaev interactions [35,36], which is another important factor that can affect the formation of magnetic topological states. Due to all these subtle interactions, $\text{CrGe}(\text{Se}, \text{Te})_3$ appears to be promising to host exotic magnetic topological states, as we are going to prove.

To explore spin structures in the Janus $\text{CrGe}(\text{Se}, \text{Te})_3$ monolayer, we first conduct parallel tempering Monte Carlo (PTMC) simulations (as detailed in the SM [28]) based on the first-principles parametrized Hamiltonian of Eq. (1) and in the absence of an external field. Figure 2 shows representative images of the spin structure at different temperatures. Note that the simulation starts from a random configuration to explore the configurational space of low-energy states. Three magnetic topological defects coexist and can be seen at 0.1 K, as shown in Fig. 2(a): skyrmion, skyrmionium, and fragmented labyrinth domains with very weak orientational order. The labyrinth pattern consists of convoluted stripes and meandering domains. Due to the large DMI, all these topological defects are found to exhibit Néel-type characteristics with a unique rotational sense. More strikingly, the size of skyrmion and skyrmionium under no magnetic field is ≈ 4.2 nm and ≈ 7.8 nm, respectively, which is less than 10 nm and thus technologically promising [37,38]. The width of the domain wall of the labyrinthine stripes is also nanometric in size, namely ≈ 3.5 nm. All these nanometer-sized spin textures can be attributed to the large $|D_1/J_1|$ ratio and uniaxial anisotropy [4,31,39,40]. As the temperature increases, thermal activation effects come into play and the labyrinth states become more dominant, as shown in Fig. 2(b). Further increasing temperature tends to break the labyrinthine domain, as demonstrated in Fig. 2(c). When the temperature is higher than $T_c \approx 20$ K, the system fully disorders to form the paramagnetic state [see Fig. 2(d) and specific heat in Fig. S1

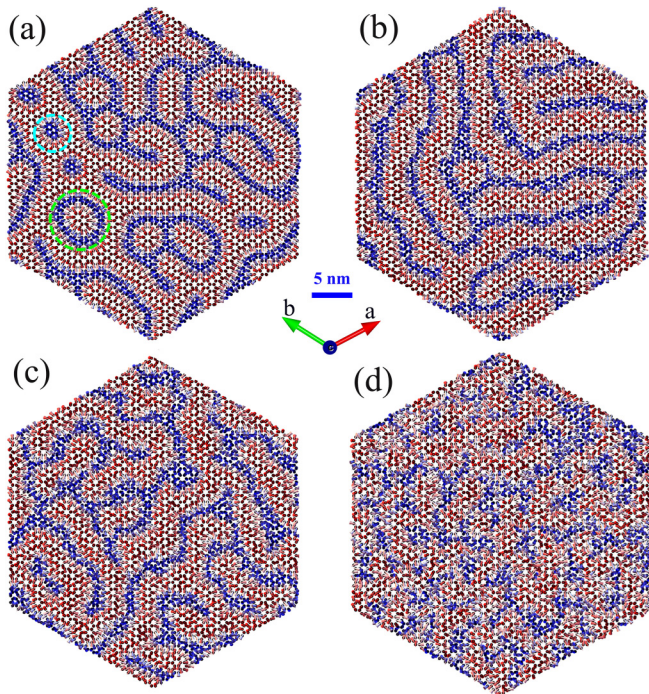


FIG. 2. The evolution of the spin texture of the $\text{CrGe}(\text{Se}, \text{Te})_3$ monolayer with increasing temperature: (a) 0.1 K, (b) 6.1 K, (c) 10.2 K, and (d) 20.3 K. The skyrmion and skyrmionium is highlighted with cyan and green circle, respectively. The red color denotes magnetic moments pointing up, while the blue color represents spins pointing into the opposite direction.

of the SM [28] for the determination of the transition towards paramagnetism].

To gain further insight into the mechanism that stabilizes these distinct topological defects at zero field, we first need to identify the true ground-state spin configuration of $\text{CrGe}(\text{Se}, \text{Te})_3$ (as detailed in the SM [28]). When first

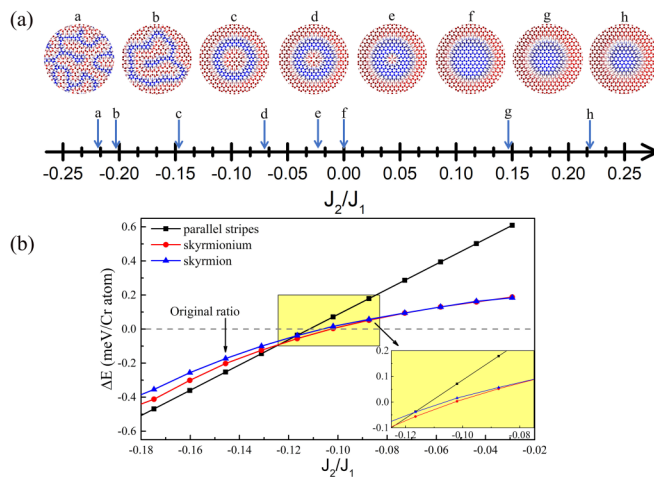


FIG. 3. (a) Frustration strength J_2/J_1 dependence of relaxed skyrmioniums with DMI, with c corresponding to the original ratio. (b) Total energy difference with respect to FM state for ideal parallel stripes, skyrmion, and skyrmionium, as a function of the frustration strength J_2/J_1 .

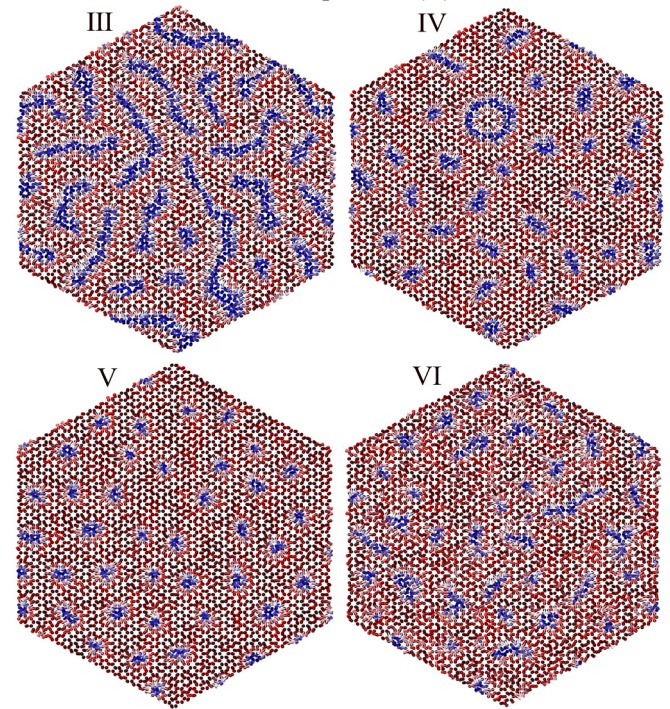
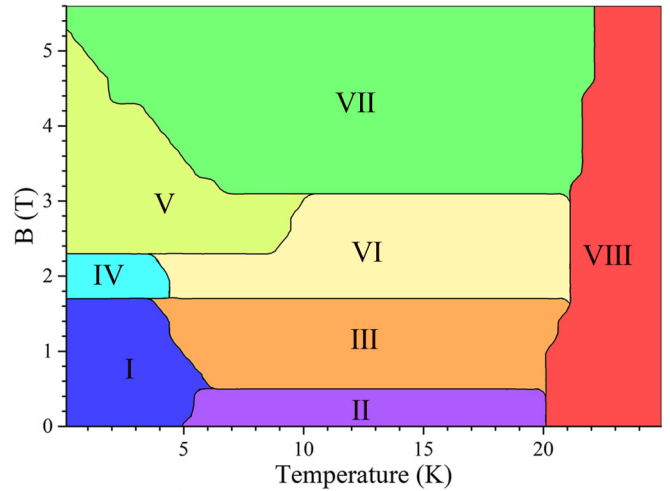


FIG. 4. Magnetic field versus temperature phase diagram of the studied $\text{CrGe}(\text{Se}, \text{Te})_3$ Janus monolayer. The phase boundaries are determined by heat capacity, magnetic susceptibility, local spin chirality, as well as snapshots. The eight phases depicted are as follows: fragmented labyrinth domain, skyrmion and skyrmionium mixed phase (I), labyrinth domain (II), fragmented labyrinth domain and skyrmion mixed phase (III), isolated skyrmion and skyrmionium mixed phase (IV), isolated skyrmion (V), hybrid skyrmion phase (VI, for which some skyrmions merge together but others remain isolated), saturated ferromagnetic state (VII), and paramagnetic state (VIII). Representative spin textures are shown for phase III ($B = 0.8$ T, $T = 7.69$ K), phase IV ($B = 1.8$ T, $T = 4.14$ K), phase V ($B = 2.4$ T, $T = 4.14$ K), and phase VI ($B = 2.4$ T, $T = 13.3$ K).

constructing by hand skyrmions, skyrmioniums, and parallel stripes and then relaxing them, the ground state is found to consist of parallel stripes with an energy of -0.253 meV/Cr atom with respect to the homogeneous FM that we chose as the reference state. The isolated skyrmion (-0.173 meV/Cr atom with respect to FM) with an optimized diameter ≈ 4.2

nm is found to be slightly higher in energy. Interestingly, the isolated skyrmionium with an exceptionally small diameter of ≈ 7.3 nm is even closer to the ground state in energy (-0.207 meV/Cr atom with respect to FM).

To better understand the microscopic origin of the aforementioned spin textures, the DMI vectors are decomposed into their $\{rpz\}$ components by using the same procedure as in our previous work [20] (as indicated in Fig. S3, the \hat{r} axis is along the Cr-Cr bond direction and thus in-plane; the \hat{p} axis is perpendicular to \hat{r} and also in-plane, and the \hat{z} axis is in the out-of-plane direction). As shown in Table SI of the SM [28], this decomposition gives $D_1 = (0, 0.689, -0.171)$ and $D_2 = (-0.142, 0.054, 0.197)$ meV. Then, we perform additional calculations by switching on one magnetic parameter component and off the others to determine the relative importance of different contributions to the stability of spin texture, as listed in Table SII. It is found that D_1^p and D_2^p both contribute to energy gains for all three Néel-type states, which is consistent with previous reports [41]. Interestingly, second NN interactions also cause considerable energy gains for all three states. This finding is in line with the fact that skyrmions can be further stabilized by exchange frustration [33]. Furthermore, the skyrmionium is found to be (meta)stable even in frustrated magnets without DMI, as also reported in Ref. [42]. However, the precise competitive mechanism between DMI and frustration to stabilize the skyrmionium has never been elucidated. To this end, we study the dependence of the frustration strength (as characterized by the J_2/J_1 ratio with J_1 being unchanged) on the stability of the skyrmionium, with DMIs taken into account, as shown in Fig. 3(a). The skyrmionium cannot be stabilized and spontaneously relaxes to skyrmion for positive J_2/J_1 (not shown here), which is when frustration is not present. When $J_2/J_1 = -0.03$, the skyrmionium starts to appear with a tiny inner skyrmion core. As frustration increases via J_2/J_1 becoming more negative and enhancing its magnitude, the size of the inner skyrmion gradually grows. Interestingly, the skyrmionium becomes distorted at $J_2/J_1 = -0.20$ and collapses to convoluted domains when further increasing the frustration. Therefore, a moderate frustrated interaction plays an important role in stabilizing skyrmionium in chiral magnets. Moreover, when we removed both NN and second-NN DMI, although skyrmionium-like patterns can exist in a small frustration range $-0.25 < J_2/J_1 < -0.20$, the FM state is more stable than skyrmionic states (as shown in Fig. S4). We also compared the total energies of the FM, skyrmion, skyrmionium, and ideal parallel stripes in the J_2/J_1 range of skyrmionium existence. As shown in Fig. 3(b), we find that skyrmionium is the most favorable stable state within a small frustration window of $-0.125 < J_2/J_1 < -0.075$.

Finally, we establish a magnetic field vs temperature phase diagram by applying an external field magnetic field \mathbf{B} pointing upwards along the out-of-plane direction. We obtain a rich phase diagram of exotic magnetic configurations, as shown in Fig. 4. In total, we identify eight different phases. At low temperature, there is a mixed domain structure consisting of fragmented labyrinth domains with very weak orientational order, as well as skyrmions and skyrmioniums [phase I in Fig. 4 and pattern in Fig. 2(a)]. The labyrinth phase (phase II) becomes dominating as the temperature increases for small fields. The magnetic field first tends to break the labyrinth domain into fragments (phase III). Further increments of magnetic field totally wipe out the labyrinth states (phases IV and V). Note that skyrmion and skyrmionium coexist in a small region marked as the cyan area (phase IV). For higher temperatures and sizable magnetic fields, the skyrmioniums vanish and skyrmions tend to merge with each other (VI). For $B > 2.3$ T (phase V), the skyrmions become more packed towards forming a skyrmion lattice. When $B > 5.3$ T, the system is completely magnetized into FM state (phase VII). Moreover, when T is larger than about 20 K, the system disorders to form a paramagnetic state, for any magnetic field (VIII).

In summary, using first-principles calculations, we propose a new Janus monolayer $\text{CrGe}(\text{Se}, \text{Te})_3$. Owing to its inherent inversion asymmetry, significant DMI is induced. The MC simulations show that spontaneous skyrmionium appear without applied magnetic field. The competition between DMI and frustration is found critical to stabilize skyrmionium. Our study thus sheds new light on exploitation of 2D vdW skyrmionic devices and provides a new platform for understanding the skyrmionium properties.

ACKNOWLEDGMENTS

This work is mostly supported by the Vannevar Bush Faculty Fellowship (VBFF) from the Department of Defense. P.C. and L.B. also acknowledge the Office of Naval Research under grant number N00014-17-1-2818. Y.N., S.P., and L.B. also thank the DARPA Grant No. HR0011727183-D18AP00010 (TEE Program). Y.Z. is supported by National Natural Science Foundation of China (NSFC 11704007) and China Scholarship Council (CSC, 201808615126). This research is also supported by the Arkansas High Performance Computing Center which is funded through multiple National Science Foundation grants and the Arkansas Economic Development Commission.

[1] S. Mühlbauer, B. Binz, F. Jonietz, C. Pfleiderer, A. Rosch, A. Neubauer, R. Georgii, and P. Böni, *Science* **323**, 915 (2009).
 [2] U. K. Roessler, A. Bogdanov, and C. Pfleiderer, *Nature (London)* **442**, 797 (2006).
 [3] S. Heinze, K. Von Bergmann, M. Menzel, J. Brede, A. Kubetzka, R. Wiesendanger, G. Bihlmayer, and S. Blügel, *Nat. Phys.* **7**, 713 (2011).
 [4] N. Nagaosa and Y. Tokura, *Nat. Nanotechnol.* **8**, 899 (2013).

[5] N. Romming, C. Hanneken, M. Menzel, J. E. Bickel, B. Wolter, K. von Bergmann, A. Kubetzka, and R. Wiesendanger, *Science* **341**, 636 (2013).
 [6] J. Zang, M. Mostovoy, J. H. Han, and N. Nagaosa, *Phys. Rev. Lett.* **107**, 136804 (2011).
 [7] W. Jiang, X. Zhang, G. Yu, W. Zhang, X. Wang, M. B. Jungfleisch, J. E. Pearson, X. Cheng, O. Heinonen, K. L. Wang *et al.*, *Nat. Phys.* **13**, 162 (2017).

- [8] K. Litzius, I. Lemesh, B. Krüger, P. Bassirian, L. Caretta, K. Richter, F. Büttner, K. Sato, O. A. Tretiakov, J. Förster *et al.*, *Nat. Phys.* **13**, 170 (2017).
- [9] J. Barker and O. A. Tretiakov, *Phys. Rev. Lett.* **116**, 147203 (2016).
- [10] W. Legrand, D. Maccariello, F. Ajejas, S. Collin, A. Vecchiola, K. Bouzehouane, N. Reyren, V. Cros, and A. Fert, *Nat. Mater.* **19**, 34 (2020).
- [11] X. Zhang, J. Xia, Y. Zhou, D. Wang, X. Liu, W. Zhao, and M. Ezawa, *Phys. Rev. B* **94**, 094420 (2016).
- [12] F. Zheng, H. Li, S. Wang, D. Song, C. Jin, W. Wei, A. Kovács, J. Zang, M. Tian, Y. Zhang *et al.*, *Phys. Rev. Lett.* **119**, 197205 (2017).
- [13] S. Zhang, F. Kronast, G. van der Laan, and T. Hesjedal, *Nano Lett.* **18**, 1057 (2018).
- [14] B. Göbel, A. F. Schäffer, J. Berakdar, I. Mertig, and S. S. Parkin, *Sci. Rep.* **9**, 1 (2019).
- [15] B. Huang, G. Clark, E. Navarro-Moratalla, D. R. Klein, R. Cheng, K. L. Seyler, D. Zhong, E. Schmidgall, M. A. McGuire, D. H. Cobden *et al.*, *Nature (London)* **546**, 270 (2017).
- [16] C. Gong, L. Li, Z. Li, H. Ji, A. Stern, Y. Xia, T. Cao, W. Bao, C. Wang, Y. Wang *et al.*, *Nature (London)* **546**, 265 (2017).
- [17] Y. Deng, Y. Yu, Y. Song, J. Zhang, N. Z. Wang, Z. Sun, Y. Yi, Y. Z. Wu, S. Wu, J. Zhu *et al.*, *Nature (London)* **563**, 94 (2018).
- [18] J. Liang, W. Wang, H. Du, A. Hallal, K. Garcia, M. Chshiev, A. Fert, and H. Yang, *Phys. Rev. B* **101**, 184401 (2020).
- [19] J. Yuan, Y. Yang, Y. Cai, Y. Wu, Y. Chen, X. Yan, L. Shen *et al.*, *Phys. Rev. B* **101**, 094420 (2020).
- [20] C. Xu, J. Feng, S. Prokhorenko, Y. Nahas, H. Xiang, and L. Bellaiche, *Phys. Rev. B* **101**, 060404(R) (2020).
- [21] M.-G. Han, J. A. Garlow, Y. Liu, H. Zhang, J. Li, D. DiMarzio, M. W. Knight, C. Petrovic, D. Jariwala, and Y. Zhu, *Nano Lett.* **19**, 7859 (2019).
- [22] B. Ding, Z. Li, G. Xu, H. Li, Z. Hou, E. Liu, X. Xi, F. Xu, Y. Yao, and W. Wang, *Nano Lett.* **20**, 868 (2019).
- [23] H. Wang, C. Wang, Y. Zhu, Z.-A. Li, H. Zhang, H. Tian, Y. Shi, H. Yang, and J. Li, *arXiv:1907.08382*.
- [24] T.-E. Park, L. Peng, X. Zhang, S. J. Kim, K. M. Song, K. Kim, M. Weigand, G. Schütz, S. Finizio, J. Raabe *et al.*, *arXiv:1907.01425*.
- [25] Y. Wu, S. Zhang, J. Zhang, W. Wang, Y. L. Zhu, J. Hu, K. Wong, C. Fang, C. Wan, X. Han *et al.*, *Nat. Commun.* **11**, 3860 (2020).
- [26] A.-Y. Lu, H. Zhu, J. Xiao, C.-P. Chuu, Y. Han, M.-H. Chiu, C.-C. Cheng, C.-W. Yang, K.-H. Wei, Y. Yang *et al.*, *Nat. Nanotechnol.* **12**, 744 (2017).
- [27] J. Zhang, S. Jia, I. Kholmanov, L. Dong, D. Er, W. Chen, H. Guo, Z. Jin, V. B. Shenoy, L. Shi *et al.*, *ACS Nano* **11**, 8192 (2017).
- [28] See Supplemental Materials at <http://link.aps.org/supplemental/10.1103/PhysRevB.102.241107> for detailed methods and further discussions on our results, which includes Refs. [35,36,43–56].
- [29] T. Moriya, *Phys. Rev.* **120**, 91 (1960).
- [30] A. Fert, V. Cros, and J. Sampaio, *Nat. Nanotechnol.* **8**, 152 (2013).
- [31] J. Sampaio, V. Cros, S. Rohart, A. Thiaville, and A. Fert, *Nat. Nanotechnol.* **8**, 839 (2013).
- [32] A. O. Leonov and M. Mostovoy, *Nat. Commun.* **6**, 8275 (2015).
- [33] S. von Malottki, B. Dupé, P. F. Bessarab, A. Delin, and S. Heinze, *Sci. Rep.* **7**, 1 (2017).
- [34] E. Oliveira, R. Silva, R. Silva, and A. Pereira, *J. Phys.: Condens. Matter* **29**, 205801 (2017).
- [35] C. Xu, J. Feng, H. Xiang, and L. Bellaiche, *npj Comput. Mater.* **4**, 57 (2018).
- [36] C. Xu, J. Feng, M. Kawamura, Y. Yamaji, Y. Nahas, S. Prokhorenko, Y. Qi, H. Xiang, and L. Bellaiche, *Phys. Rev. Lett.* **124**, 087205 (2020).
- [37] S. Meyer, M. Perini, S. von Malottki, A. Kubetzka, R. Wiesendanger, K. von Bergmann, and S. Heinze, *Nat. Commun.* **10**, 1 (2019).
- [38] Y. Fujishiro, N. Kanazawa, and Y. Tokura, *Appl. Phys. Lett.* **116**, 090501 (2020).
- [39] A. K. Behera, S. S. Mishra, S. Mallick, B. B. Singh, and S. Bedanta, *J. Phys. D: Appl. Phys.* **51**, 285001 (2018).
- [40] A. B. Butenko, A. A. Leonov, A. N. Bogdanov, and U. K. Röbler, *Phys. Rev. B* **80**, 134410 (2009).
- [41] G. Yin, Y. Li, L. Kong, R. K. Lake, C.-L. Chien, and J. Zang, *Phys. Rev. B* **93**, 174403 (2016).
- [42] J. Xia, X. Zhang, M. Ezawa, O. A. Tretiakov, Z. Hou, W. Wang, G. Zhao, X. Liu, H. T. Diep, and Y. Zhou, *Appl. Phys. Lett.* **117**, 012403 (2020).
- [43] Y. Miyatake, M. Yamamoto, J. Kim, M. Toyonaga, and O. Nagai, *J. Phys. C: Solid State Phys.* **19**, 2539 (1986).
- [44] A. Togo and I. Tanaka, *Scr. Mater.* **108**, 1 (2015).
- [45] S. Baroni, S. De Gironcoli, A. Dal Corso, and P. Giannozzi, *Rev. Mod. Phys.* **73**, 515 (2001).
- [46] G. Kresse and D. Joubert, *Phys. Rev. B* **59**, 1758 (1999).
- [47] H. Xiang, C. Lee, H.-J. Koo, X. Gong, and M.-H. Whangbo, *Dalton Trans.* **42**, 823 (2013).
- [48] C. Xu, B. Xu, B. Dupé, and L. Bellaiche, *Phys. Rev. B* **99**, 104420 (2019).
- [49] H. J. Xiang, E. J. Kan, S.-H. Wei, M.-H. Whangbo, and X. G. Gong, *Phys. Rev. B* **84**, 224429 (2011).
- [50] H. J. Xiang, S.-H. Wei, and M.-H. Whangbo, *Phys. Rev. Lett.* **100**, 167207 (2008).
- [51] W. Kohn and L. J. Sham, *Phys. Rev.* **140**, A1133 (1965).
- [52] P. E. Blöchl, *Phys. Rev. B* **50**, 17953 (1994).
- [53] A. Togo, F. Oba, and I. Tanaka, *Phys. Rev. B* **78**, 134106 (2008).
- [54] P. S. Wang and H. J. Xiang, *Phys. Rev. X* **4**, 011035 (2014).
- [55] G. Menichetti, M. Calandra, and M. Polini, *2D Mater.* **6**, 045042 (2019).
- [56] S. L. Dudarev, G. A. Botton, S. Y. Savrasov, C. J. Humphreys, and A. P. Sutton, *Phys. Rev. B* **57**, 1505 (1998).